



Adaptive SVSF-KF estimation strategies based on the normalized innovation square metric and IMM strategy

Jacob Goodman^b, Waleed Hilal^{a,*}, S. Andrew Gadsden^a, Charles D. Eggleton^b

^a Department of Mechanical Engineering at McMaster University, Hamilton, ON, Canada

^b Department of Mechanical Engineering at the University of Maryland, Baltimore County, Baltimore, MD, USA

ABSTRACT

The smooth variable structure filter (SVSF) is highly robust to modeling uncertainty and unknown disturbances. Recent developments to the SVSF have allowed for the creation of an adaptive estimation scheme termed the SVSF-KF, which balances the optimality of the Kalman filter (KF) with the robustness of the SVSF. The approach utilizes the KF estimate during normal operation, and utilizes the robust SVSF gain to estimate the states during the presence of a fault. However, the gain adaptation involved in detecting a fault and switching between the KF and SVSF estimates suffers from several limitations, including unwanted chattering. In this work, we review the original SVSF-KF approach and present two novel SVSF-KF strategies based on the normalized innovation square metric and the interacting multiple model strategy to address these limitations. Experimental simulations involving a simple harmonic oscillator subject to a fault condition are conducted, which verify the effectiveness of our proposed approaches.

Index Terms—Smooth variable structure filter, Kalman filter, adaptive filtering, sliding mode concepts, interacting multiple models, modeling uncertainty, robust estimation.

1. Introduction

An estimator's performance in the face of modeling uncertainty and system change is of particular interest in much of the existing literature. The Kalman filter (KF), which depends on an accurate system model, can be sensitive to uncertainty – and yield poor estimates or ultimately fail [1]. This is a real concern in many applications. Oftentimes, the complete dynamics of a system is not well understood, and only limited modeling is possible. Even in situations where an accurate model is available, many systems change – either due to a fault condition, or because the system's nature causes it to operate in more than one mode [2].

The smooth variable structure filter (SVSF) is a relatively new estimation algorithm (at least compared to the KF) which was proposed in 2007 and is based on sliding mode concepts [3,4,5,6,7]. The SVSF is structurally similar to the KF in its predictor-corrector arrangement, but it is a sub-optimal estimator. The SVSF gain uses a nonlinear switching action to drive the state estimates to within a region of the true states, known as the existence subspace. The width of the existence subspace is unknown but assumed to be bounded and relative to the level of uncertainties and noise present in the system and measurements. Once

within the existence subspace, the state estimates are forced to remain there throughout the estimation process. Because of the nature of this switching action, an artificial high-frequency noise known as chattering is introduced. To mitigate the effects of this chattering, a smoothing boundary layer (SBL) term is added. The width of the smoothing boundary layer determines the extent to which the chattering is attenuated, but at the same time can result in degradation of the filter's overall performance in terms of estimation error [4,8].

Despite its lack of optimality, the SVSF has been shown to be highly robust to modeling uncertainty and system change, while still providing some reduction of measurement noise [5]. The SVSF proof of stability may be found in the Appendix. These properties render the SVSF an attractive option for many applications where sudden system change is a real concern. Indeed, the SVSF has been an active area of academic research with numerous improvements and applications advanced in the few years since its release [9–32]. The SVSF, unlike many estimation schemes, does not require a covariance calculation in its recursion process. This fact makes the SVSF naturally applicable to many nonlinear systems requiring only that the measurement model be linear and the nonlinear system equations be 'smooth' [4]. An early advancement to the SVSF was the derivation of a covariance calculation [33,34]. While not needed for the essential estimation process, it provides a useful measure of the estimator's performance, and more importantly, opens the door to the SVSF's integration with other existing algorithms [35].

* Corresponding author.

E-mail address: hilalw@mcmaster.ca (W. Hilal).

One of the first applications of the new SVSF covariance term was to derive an optimal time-varying smoothing boundary layer width (VBL) [34]. Prior to this approach, a conservative problem-specific fixed width for the SBL was used. The goal of the VBL was to provide an optimal amount of smoothing to the SVSF estimate. With the optimal VBL however, it was discovered that the SVSF was reduced to the KF, and its robust properties lost. Other sub-optimal VBL approaches were also put forward in the literature [8,36].

Given the optimal VBLs reduction of the SVSF to a KF, a hybrid approach was proposed. Termed the SVSF-KF, the resultant is an estimation strategy that would provide the more optimal KF estimate during normal system operation and that of the SVSF in the presence of a fault. The VBL was used as a detection/switching mechanism, where a sudden increase in the VBL width beyond a designer specified threshold would control activation of the SVSF gain. The SVSF-KF was successfully demonstrated in multiple cases [16,19,34,37–42], and several non-linear extensions were advanced based on the extended Kalman filter (EKF), the unscented Kalman filter (UKF), and the cubature Kalman filter (CKF), termed SVSF-EKF, SVSF-UKF, and SVSF-CKF respectively.

In this paper, we present a closer study of the SVSF-KF, particularly the mechanism to switch between the KF and SVSF estimates. Some issues have been noted with the current VBL-based methodology, specifically that chattering is often observed in the state estimates. Due to this chattering, the VBL at times fails to provide ongoing indication of a fault, resulting in an inability to switch to the SVSF gain. This paper aims to address and remedy this problem. In response, we propose two new alternative approaches to remedy these problems. The first exchanges the VBL with a simple threshold approach based on the normalized innovation square (NIS). In the second approach, we use the more sophisticated framework of the interacting multiple model (IMM) estimator. A NIS-driven adaptive gain formulation of the SVSF-KF as well as one based on the IMM are hypothesized to have several advantages over the existing SVSF-KF – as shall be highlighted and discussed in later sections of this paper.

This paper is organized as follows. In section II, we provide a basic mathematical background behind the KF, as well as the SVSF formulation with covariance, and finally the SVSF-KF. We also summarize some of the issues with the existing SVSF-KF strategy and its use of the VBL to detect system change. In section III, we present two new approaches for detecting system change. In section IV, we present our simulation results and discussion, followed by the overall conclusions of this research paper in section V.

2. Estimation strategies

2.1. The Kalman filter

A linear system can be expressed in discrete state representation form as follows [43,34,44,45]:

$$\mathbf{x}_{k+1} = \mathbf{A}\mathbf{x}_k + \mathbf{B}\mathbf{u}_k + \mathbf{w}_k \quad (1)$$

$$\mathbf{z}_k = \mathbf{H}\mathbf{x}_k + \mathbf{v}_k \quad (2)$$

where \mathbf{x} is the system state vector, \mathbf{A} is the discretized linear system model matrix, \mathbf{B} is the input gain matrix, \mathbf{u} is the input vector, \mathbf{w} is the system noise, \mathbf{z} is the measurement vector, \mathbf{H} is the linear measurement matrix, \mathbf{v} represents the measurement noise, and k represents the current timestep.

The KF assumes that the system model is well-known and linear, the initial states are known, and the measurement and system noise is white with zero mean and known respective covariance matrices (i.e., normal and Gaussian) [44]. The KF works as a predictor-corrector; the system model is used to obtain an *a priori* or predicted estimate of the states, whereupon measurements combined with the Kalman gain matrix are

used to apply a correction term to create an *a posteriori* or updated state estimate.

The *a priori* state estimate is first computed using the process model, as can be seen in (3). Then, the *a priori* state covariance matrix is calculated based on the process model and the associated modeling noise covariance matrix \mathbf{Q}_k , as shown in (4):

$$\hat{\mathbf{x}}_{k+1|k} = \mathbf{A}\hat{\mathbf{x}}_{k|k} + \mathbf{B}\mathbf{u}_k \quad (3)$$

$$\hat{\mathbf{P}}_{k+1|k} = \mathbf{A}\mathbf{P}_{k|k}\mathbf{A}^T + \mathbf{Q}_k \quad (4)$$

The Kalman gain computation in (5) is based on (4), and is then used to update the state estimate in (6):

$$\mathbf{K}_{k+1} = \mathbf{P}_{k+1|k}\mathbf{H}^T\mathbf{S}_{k+1}^{-1} \quad (5)$$

$$\hat{\mathbf{x}}_{k+1|k+1} = \hat{\mathbf{x}}_{k+1|k} + \mathbf{K}_{k+1}\mathbf{v}_{k+1} \quad (6)$$

where \mathbf{v} and \mathbf{S} are two important terms known as the innovation (or residual), and the innovation covariance, respectively. In the equations below, \mathbf{R} is the measurement noise covariance.

$$\mathbf{v}_{k+1} = \mathbf{z}_k - \mathbf{H}\mathbf{A}\hat{\mathbf{x}}_{k+1|k} \quad (7)$$

$$\mathbf{S}_{k+1} = \mathbf{H}\mathbf{P}_{k+1|k}\mathbf{H}^T + \mathbf{R}_{k+1} \quad (8)$$

The innovation, from (7), represents the difference between the actual measurements and the *a priori* estimate of the measurements. The innovation covariance, as in (8), characterizes the uncertainty in the measurement predictions. These two terms provide an important insight into the estimation process and are often used to assess the filter's overall estimation ability.

The *a posteriori* state error covariance matrix is then calculated in (9), and the process repeats iteratively:

$$\mathbf{P}_{k+1|k+1} = (\mathbf{I} - \mathbf{K}_{k+1}\mathbf{H})\mathbf{P}_{k+1|k}(\mathbf{I} - \mathbf{K}_{k+1}\mathbf{H})^T + \mathbf{K}_{k+1}\mathbf{R}_{k+1}\mathbf{K}_{k+1}^T \quad (9)$$

where \mathbf{I} is the identity matrix. In a successful application of the KF, the state estimates will rapidly converge, providing the optimal statistical estimate based on the given information. The *a posteriori* covariance update in (9) is known as the 'Joseph covariance form' and is often preferred due to its superior numerical characteristics. The Joseph form ensures that the covariance update remains positive-definite, a critical condition in the estimation process to produce meaningful results [44].

2.2. The smooth variable structure filter

The SVSF uses a nonlinear switching gain to drive the state estimates to within a specific boundary of the true states – known as the 'existence subspace.' The width of the existence subspace fluctuates with time and is a function of the various

System uncertainties – hence, its exact width at any point in time is unknown [4]. If a bound can be placed on the overall system uncertainties, a bound for the existence subspace can be determined as well. During the initial estimation period, states outside existence subspace are forced toward the existence subspace by means of the SVSF gain. Once within the existence subspace, the estimates will be confined to the subspace throughout the estimation process, as shown in Fig. 1.

Due to the nature of the SVSF's formulation and the nonlinear switching gain, the state estimates are sensitive to an effect known as chattering. Unlike the KF, which under ideal conditions will converge to the minimum mean squared state estimate (MMSE) given a set of measurements, the SVSF only converges to the previously mentioned existence subspace.

Within this subspace, the state estimates chatter about the true states. Chattering in the *a posteriori* estimate eventually decays with time until the estimated state converges to the measured state. As such, the SVSF can be very sensitive to measurement noise. To reduce the effects

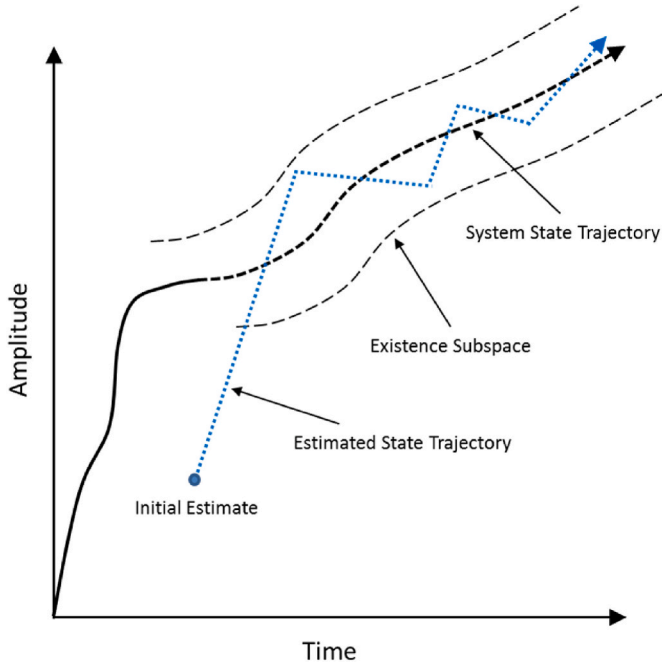


Fig. 1. Basic concept of the sliding boundary layer in SVSF [46,13].

of chattering and sensitivity to measurement noise, a SBL is applied to the estimate. A SBL width is specified (one for each state) such that the corrective action of the SVSF gain is interpolated based on this width and the *a priori* estimation error [4,8]. As noted, in the initial formulation of the SVSF the SBL width was defined to be constant throughout the estimation process. In more recent versions of the SVSF, various VBL approaches have been proposed [8,34,36,47]. The width of this boundary layer generally determines the overall performance of the SVSF. Too wide and the estimates become less accurate and/or diverge. Too small and chattering can become dominant, and the SVSF simply returns the measured state as its estimate.

The SVSF can be applied to both linear systems modeled as in (1) or non-linear systems expressed as follows in (10). Note the measurement equation (11) must be linear or linearizable.

$$\mathbf{x}_{k+1} = \mathcal{F}(\mathbf{x}_k, \mathbf{u}_k, \mathbf{w}_k) \quad (10)$$

$$\mathbf{z}_k = \mathbf{H}\mathbf{x}_k + \mathbf{v}_k \quad (11)$$

An important prerequisite of the SVSF is that the system in question be differentiable as well as observable. In addition, a full rank linear measurement matrix \mathbf{H} is required for the SVSF to operate. In situations where full measurements are not available, an augmented measurement matrix can be constructed using a reduced order observer strategy. For nonlinear measurement equations, linearization strategies like those used in the EKF can be employed.

The SVSF process is presented next. Note that the procedure is the same for linear or nonlinear systems and measurements. An *a priori* state estimate is determined in (12), similar to the KF process. The estimated *a priori* measurements are then calculated by (13) as follows:

$$\hat{\mathbf{x}}_{k+1|k} = \mathbf{A}\hat{\mathbf{x}}_{k+1|k} + \mathbf{B}\mathbf{u}_k \quad (12)$$

$$\hat{\mathbf{z}}_{k+1|k} = \hat{\mathbf{H}}\hat{\mathbf{x}}_{k+1|k} \quad (13)$$

If the measurement is nonlinear, it can be linearized to form a linearized measurement matrix as per the EKF process. The *a priori* output error estimate is calculated next as follows:

$$\mathbf{e}_{z_{k+1|k}} = \mathbf{z}_k - \hat{\mathbf{z}}_{k+1|k} \quad (14)$$

The SVSF gain \mathbf{K}_{k+1} is calculated based on the *a priori* and *a posteriori*

output error estimates. The *a priori* state estimate is then updated to the *a posteriori* state estimate using the SVSF gain:

$$\hat{\mathbf{x}}_{k+1|k+1} = \hat{\mathbf{x}}_{k+1|k} + \mathbf{K}_{k+1} \quad (15)$$

The *a posteriori* measurements are then calculated per (16) as follows:

$$\hat{\mathbf{z}}_{k+1|k+1} = \hat{\mathbf{H}}\hat{\mathbf{x}}_{k+1|k+1} \quad (16)$$

The *a priori* output error estimate is updated to the *a posteriori* output error estimate. The process then repeats iteratively.

$$\mathbf{e}_{z_{k+1|k+1}} = \mathbf{z}_k - \hat{\mathbf{z}}_{k+1|k+1} \quad (17)$$

The SVSF gain is derived based on Lyapunov stability condition [48]. It can be shown that to achieve a stable estimation process, the estimation error must be reduced with each time step. A gain which meets these conditions can be shown to be:

$$\mathbf{K} = \hat{\mathbf{H}}^+ \left(|\mathbf{e}_{z_{k+1|k}}| + \gamma |\mathbf{e}_{z_{k|k}}| \right) \circ \text{sign} \left(\mathbf{e}_{z_{k+1|k}} \right) \quad (18)$$

where $+$ denotes the pseudo inverse, \circ denotes the Schur product, and γ is a diagonal scalar matrix such that $0 < \gamma_{ii} < 1$. As mentioned, to reduce the effects of chattering, as well as improve the overall quality of the state estimates, an SBL with width Ψ can be introduced to the SVSF gain calculation as follows:

$$\mathbf{K} = \hat{\mathbf{H}}^+ \left(|\mathbf{e}_{z_{k+1|k}}| + \gamma |\mathbf{e}_{z_{k|k}}| \right) \circ \text{sat} \left(\mathbf{e}_{z_{k+1|k}}; \Psi \right) \quad (19)$$

Note that the sign function in (18) has been replaced with a saturation term in (19). For *a priori* errors smaller than the SBL width, the SVSF gain is interpolated. If the *a priori* error grows outside this bound, the full nonlinear switching gain is used. The saturation function can be defined element-wise for a given error vector \mathbf{e} and SBL width Ψ as follows [49]:

$$\text{sat}_i(\mathbf{e}, \Psi) = \begin{cases} (e_i/\psi_i) & \text{for } |e_i/\psi_i| < 1 \\ \text{sign}(e_i/\psi_i) & \text{for } |e_i/\psi_i| \geq 1 \end{cases} \quad (20)$$

It can thus be seen that the SVSF presented in Ref. [4] does not require or depend on a covariance term. The filtering qualities of the SVSF are essentially due to the action of the SBL reducing the energy of the measurement noise – which works under the assumption that the provided the noise is white. While.

This method is not optimal in a classical sense, the SVSF can provide good noise reduction capabilities while remaining robust to modeling uncertainty. Certainly, a trade-off exists between optimality and robustness to uncertainties and disturbances.

To incorporate a covariance for the purposes of providing a measure of estimation uncertainty, a revised form of SVSF update was proposed [34]:

$$\hat{\mathbf{x}}_{k+1|k+1} = \hat{\mathbf{x}}_{k+1|k} + \mathbf{K}_{k+1} \mathbf{e}_{k|k-1} \quad (21)$$

The SVSF gain according to this formulation becomes slightly more complicated:

$$\mathbf{K}_{k+1} = \hat{\mathbf{H}}^+ \text{diag} \left[\left(\gamma |\mathbf{e}_{z_{k|k}}| + |\mathbf{e}_{z_{k+1|k}}| \right) \circ \text{sat} \left(\mathbf{e}_{z_{k+1|k}}; \Psi \right) \right] \left[\text{diag} \left(\mathbf{e}_{z_{k+1|k}} \right) \right]^{-1} \quad (22)$$

In this form, a covariance derivation similar in structure to that of the Kalman filter is obtained. The SVSF *a priori* and *a posteriori* covariance calculation is determined respectively to be:

$$\mathbf{P}_{k+1|k} = \mathbf{A}\mathbf{P}_{k|k}\mathbf{A}^T + \mathbf{Q}_k \quad (23)$$

$$\mathbf{P}_{k+1|k+1} = (\mathbf{I} - \mathbf{K}_{k+1}\mathbf{H})\mathbf{P}_{k+1|k}(\mathbf{I} - \mathbf{K}_{k+1}\mathbf{H})^T + \mathbf{K}_{k+1}\mathbf{R}\mathbf{K}_{k+1}^T \quad (24)$$

Note that the covariance structure is identical to that of the Kalman filter. While the basic structure is the same, the SVSF covariance will differ from that of the Kalman filter, on account of the SVSF gain defined in (22).

In the VBL strategy proposed in Ref. [34], the SVSF covariance is to be used to determine an optimal SBL width at each timestep. Using the form of the SVSF gain expressed in (22), and considering only the region within the saturation limits, the SVSF gain can also be written as:

$$K = H^{-1} \bar{A} \Psi^{-1} \quad (25)$$

where:

$$\bar{A} = \text{diag} \left[\left(|e_{z_{k+1|k}}| + \gamma |e_{z_{k|k}}| \right) \right] \quad (26)$$

Using the gain in the form of (25), the proposed optimal SBL width is the one which minimizes the trace of the *a posteriori* covariance at each time step. This is determined to be [34]:

$$\Psi = \left(\frac{\bar{A}^{-1} H P_{k+1|k} H^T}{H P_{k+1|k} H^T + R} \right)^{-1} \quad (27)$$

It is noted that by incorporating the above optimal VBL into the SVSF gain, the SVSF gain reduces to the Kalman gain [34,50]. It was thus concluded that in a linear case, the optimal smoothing boundary layer reduces the SVSF to the Kalman filter, and thus the robust switching effect of the SVSF is lost.

2.3. The SVSF-KF strategy

While the VBL if directly implemented in the SVSF results in reduction to the KF, the VBL nonetheless provides a useful indication of a system fault. During normal operation, the VBL generally converges to a size proportional to the amount of assumed process noise. In the presence of a system change the VBL will rapidly expand. With this in mind, a hybrid strategy was proposed to combine the SVSF and KF using the VBL as a Mechanism to detect system change [51].

During normal operation, the VBL is expected to remain bounded to within a fixed region. In the presence of a system change, the VBL will begin to grow beyond this bound. In setting up the filter, the designer chooses a fixed VBL threshold based on the approximate level of noise or uncertainties present. This threshold is used to determine when the filter switches to the SVSF gain. The overall hybrid strategy is illustrated in Figs. 2 and 3.

2.4. Observations on the SVSF-KF strategy

In further exploring the SVSF-KF strategy, it has been discovered that under certain conditions, the calculated VBL will fail to provide an ongoing indication of a sustained fault condition. The gain switching approach results in alternatively updating the *a posteriori* state estimate with either the KF gain or the SVSF gain. The VBL width, being highly coupled to the

Previously estimated state, will thus drop rapidly following an SVSF gain update, and remain below the triggering threshold until sufficient time has passed for the VBL to regrow. The result of this behaviour is that during an ongoing fault, the SVSF-KF will only sporadically update

the state using the SVSF gain, and otherwise maintain operation with the less robust KF gain.

To illustrate, we shall consider an underdamped simple harmonic oscillator subject to a fault condition. The system's state space equations can be expressed as:

$$\begin{bmatrix} \dot{x} \\ \dot{v} \end{bmatrix} = \begin{bmatrix} 0 & 1 \\ -\frac{k}{m} & -\frac{c}{m} \end{bmatrix} \begin{bmatrix} x \\ v \end{bmatrix} \quad (28)$$

where k is the spring constant, m is the mass, c is the damping coefficient, and x and v are the position and velocity states, respectively.

We simulate this system with an initial mass of 15 kg, 5 N/m spring constant, and 0.5 Ns/m damping coefficient. After 30 seconds, a sudden system change occurs and the mass increases to 35 kg and the damping coefficient to 2 Ns/m. Artificial measurement noise is simulated that is of Gaussian distribution with zero mean and a variance of 0.001, and otherwise, we assume no significant process noise.

The behaviour of the VBL calculated by the SVSF-KF estimation process throughout the simulation is shown in Fig. 4. The VBL in this simulation is based on the position state, and the fault detection threshold was set to a value of 50. This threshold value was manually determined through trial and error and demonstrated the lowest root mean squared error (RMSE) of the state estimate. It can be seen from Fig. 4 that the VBL can detect the onset of the fault or modeling change by rapidly growing past the threshold, thus triggering the activation of the SVSF gain. The modeling change is detected within 2 s of its occurrence. However, as anticipated, the activation of the SVSF gain results in the VBL to rapidly drop below the detection threshold. The VBL is not able to compensate for this drop immediately, and instead requires time to grow beyond the threshold again. Consequently, the SVSF gain is triggered sporadically, despite the continuous presence of the system fault at 30 s, as demonstrated clearly by the gain activation plot in Fig. 5. Furthermore, it is evident from this figure that the SVSF gain was only triggered three times throughout the entirety of the fault's presence. The obvious remedy to this problem may be to lower the detection threshold of the VBL from 50. However, this may exacerbate the effects of the chattering as the VBL displays more volatile behaviour at lower detection thresholds. This may result in more unwanted chattering near the detection threshold, and as such more rapid triggering of the activation gain.

Fig. 6 shows a plot of the SVSF-KF position state estimate. As can be seen, the filter estimates diverge and fail to track the states upon the introduction of the fault at the 30th second. While it may be possible to further adjust the VBL threshold according to the observed phenomena, the underlying problem remains unresolved. The coupling of the VBL width to the most recent state estimate renders it sensitive to the intrinsic gain-switching approach utilized by the SVSF-KF.

3. Proposed SVSF switching methods

While the VBL-based SVSF-KF may be suitable in some cases,

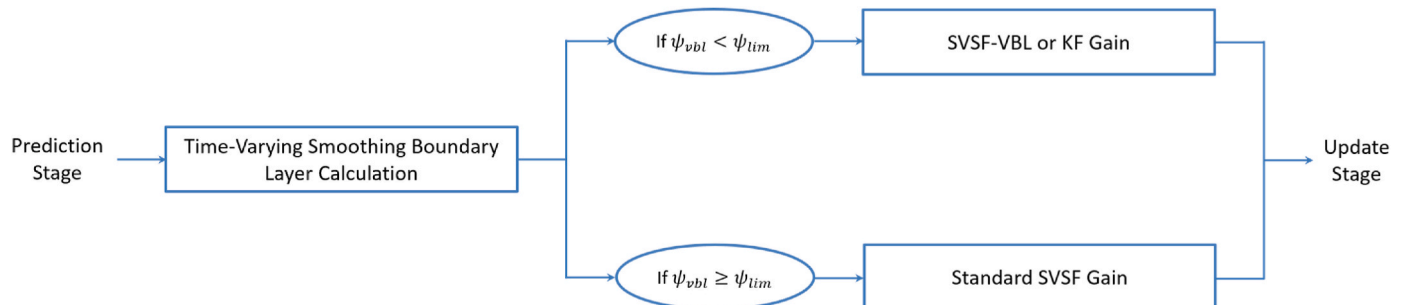


Fig. 2. Overall procedure of the SVSF-KF strategy with the VBL.

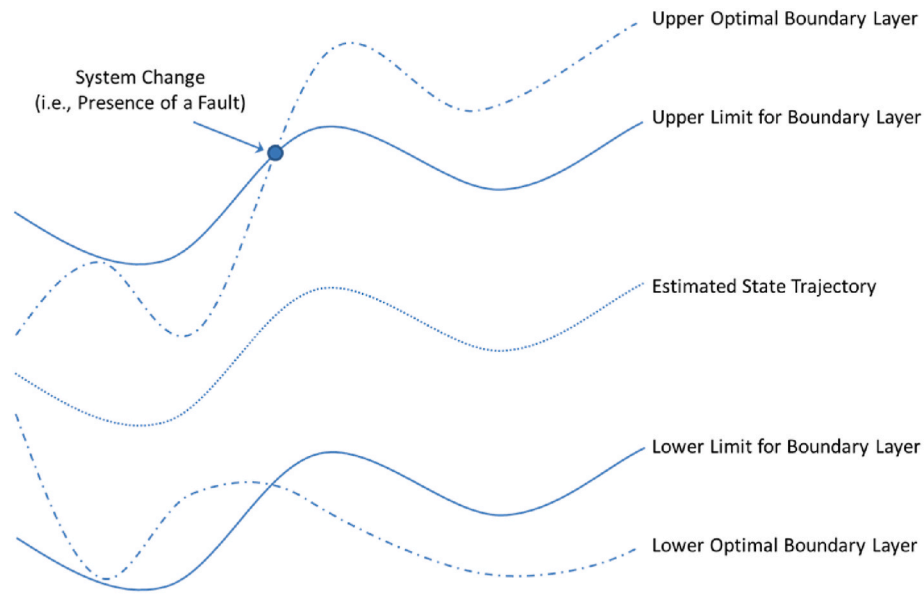


Fig. 3. Behaviour of the time-varying smoothing boundary layer under faulty conditions.

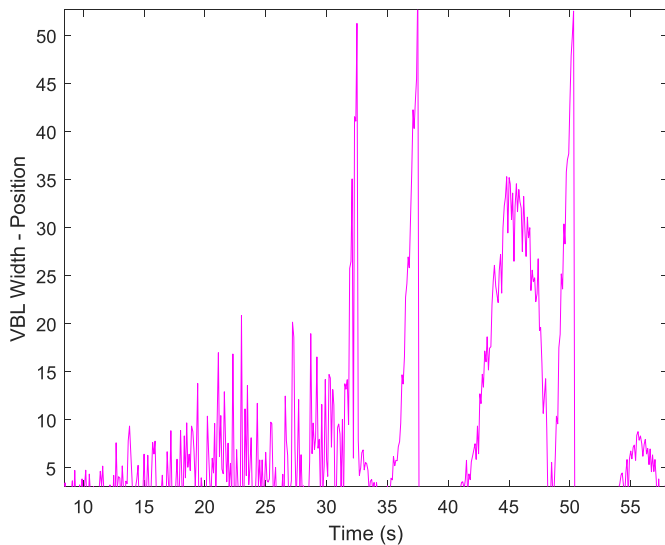


Fig. 4. VBL computed by the SVSF-KF for the position state.

alternative approaches to the detection strategy may prove to improve the SVSF-KF’s versatility across a wider range of circumstances. Although the concept of adaptively switching between an optimal KF estimate and a robust SVSF estimate has great potential, the limitations of the VBL-based detection approach must be addressed.

In response to this issue, we propose and consider two general alternatives to the existing VBL-based SVSF-KF. The first alternative involves an adaptive gain adjustment, just as the existing approach, albeit using a different mechanism for detecting the system change. The second alternative makes use of a multiple model approach, whereby the KF and SVSF estimate are independently calculated, and a framework is subsequently used to choose between or weight each of the estimates for the final output estimate.

In the first alternative, several mechanisms exist in the literature which may be considered. In this paper, we propose using the NIS and a basic threshold approach for the SVSF-KF. In the second alternative, we investigate and explore using the framework of the IMM estimator. The theory and methodology of both approaches will be covered in the next subsections.

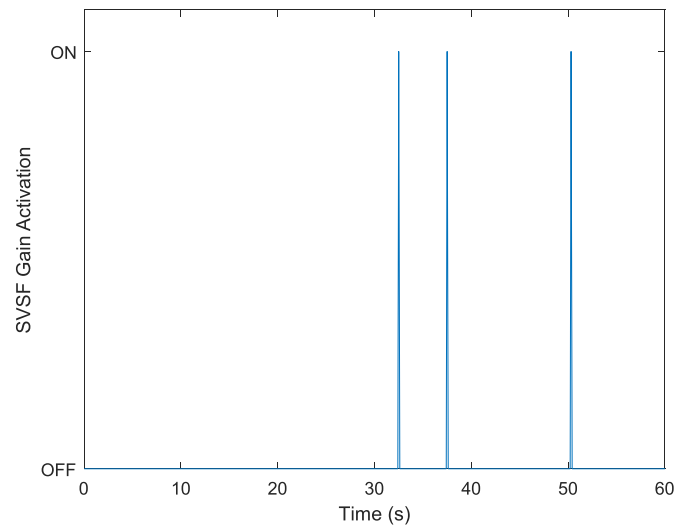


Fig. 5. SVSF-KF gain activation plot.

3.1. Normalized innovation square

The NIS is simply the square innovation vector at a given time-step, normalized by the innovation covariance. It can be expressed as follows in (29):

$$r_k = \nu_k^T S_k^{-1} \nu_k \tag{29}$$

Under the assumption of white Gaussian noise, with an accurately modeled system, a Kalman filter’s innovations are characterized by several important statistical properties. These properties of the innovations are that they are white, zero means and have a known covariance. When the filter’s model no longer accurately represents the system’s dynamics in reality, the innovations will violate these conditions. Consequently, the innovations will, in many cases, begin to grow, and thus can be used a means of detecting filter divergence [43,45,52, 53].

In this paper, we shall consider the basic threshold approach outlined in Ref. [43] for target maneuver detection. In tracking filters, a target maneuver represents a sudden change to the system model, which if

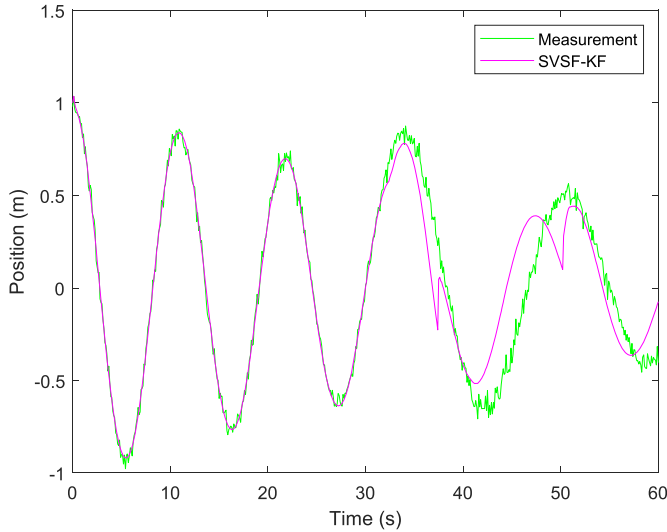


Fig. 6. Measurement and SVSF-KF estimate of the position state.

unaccounted for can lead to filter divergence. Methods used for target maneuver detection are readily applicable to other estimation applications where system change is a concern.

An NIS-based SVSF-KF involves monitoring the innovations, such that if they grow beyond a designer defined limit, a system change is assumed and the SVSF gain is triggered [53]. A reasonable threshold can be defined based on the knowledge that the NIS in an optimal, matched filter, and characterized by a chi-squared distributed with the number of degrees of freedom equal to the number of measurements N .

$$\mathbf{r} \sim \chi_N^2 \quad (30)$$

The robustness can further be improved by averaging a sequence of the innovation history. This will help smooth out any ‘noise’ in the innovations and avoid false detections. In addition, to avoid an erratic switching effect across a single threshold line, two thresholds with a hysteresis approach can be arranged: a higher ‘on’ threshold such that false triggers of the SVSF are avoided, and a lower ‘off’ threshold, to be triggered once the innovations drop back to normal.

Two basic sequence averaging techniques may be considered: the sliding window average, and the fading memory average. In the sliding window average, the most recent w innovations are averaged, with all prior innovations being ignored. In a fading memory average, the entire innovation history is included, with the more distant innovations weighted exponentially lower. The weights are determined by a forgetting factor α where $0 < \alpha < 1$.

The sliding window and fading memory average approaches can be expressed mathematically in (31) and (32), respectively [43,34]:

$$\mathbf{r}_k^w = \sum_{j=k-w+1}^k \mathbf{r}_j \quad (31)$$

$$\mathbf{r}_k^\alpha = \alpha \mathbf{r}_{k-1}^\alpha + \mathbf{r}_k \quad (32)$$

In our studies, we make use of the fading memory average. In an optimally modeled filter, the fading memory average of the NIS will also have an approximately chi-squared distribution with number of degrees of freedom related to N and α as follows [43]:

$$dof\chi = \frac{N}{1-\alpha} \quad (33)$$

The thresholds can then be defined based on an appropriate chi-squared tail probability. For example, a system with three states and a memory factor of $\alpha = 0.965$, will result in an expected chi-squared distribution with 92°-of-freedom. A tail probability of 0.001, reflecting

an unexpected innovation sequence, would translate into an ‘on’ threshold of about 140.

3.2. Interacting multiple model

The NIS threshold approach keeps the essential structure of the SVSF-KF the same – an adaptive gain with a fault detection mechanism. A structurally different approach is the multiple model method, where independent filter estimates are calculated, and a decision framework is used to pick or weigh between the most likely estimate.

In [51] we considered the use of a MMAE framework to develop an improved SVSF-KF. With the MMAE approach, the KF and SVSF filters are run in parallel, completely independent of one another. Both filters are equipped with identical system models. A Bayesian framework based on Gaussian likelihood functions of the innovation sequence is used to assess the probability of any given filter being correct. These probabilities are then used to weight each of the respective individual estimates to form the final output estimate.

The MMAE approach was shown to be effective in detecting the onset of a modeling change, and quickly switching from the KF estimate to the SVSF estimate. The MMAE SVSF-KF was also effectively able to track the system states in optimal fashion prior to the onset of the fault and did not exhibit any divergence after onset of the fault. However, the MMAE has some limitations, mainly that it is not well suited for systems which tend to exhibit mode switching [43,54,55]. Furthermore, the MMAE approach displayed significant delay in its ability to detect a fault or system change compared to the existing SVSF-KF approach. Ideally, it is desirable to have an SVSF-KF that can adaptively adjust to the system’s behaviour as needed, alternately switching between the KF and SVSF.

To this effect, we consider the IMM estimator [43]. The IMM is designed to dynamically switch between a set of potential system models as time progresses. The IMM is a popular approach, particularly in target tracking applications, and has been shown to be very effective [43,46]. With the IMM approach, multiple system/noise models are defined across the range of possible system behaviour. Special care must be taken in choosing the models and the number to adopt, as having more models does not necessarily improve performance, and can add to the computational cost. For the purposes of this study, we will not be using the IMM to switch between two different system models, but rather two different filtering methods – the KF and SVSF. Both the internal KF and SVSF shall use the exact same system model. The IMM will be used to dynamically detect system change and choose the best estimation approach. While using an IMM is much more computationally intensive than the NIS threshold approach, it may prove more robust.

The IMM works under the assumption that the transition from one system mode to another can be modeled as a Markov process with known, time invariant, mode transition probabilities. The IMM algorithm consists of five basic steps in its recursion, which is then concluded by a final output update [43,34,56]. First, the mixing probabilities $\mu_{ij,k|k}$ are calculated as per (34), which signify the probability that the system was in mode M_i at the previous time step and in mode M_j at the current time step, where $i, j = 1, \dots, r$ for r number of possible modes:

$$\mu_{ij,k|k} = \frac{1}{\bar{c}_j} p_{ij} \mu_{i,k} \quad (34)$$

$$\bar{c}_j = \sum_{i=1}^r p_{ij} \mu_{i,k} \quad (35)$$

where p_{ij} are the mode transition probabilities, $\mu_{i,k}$ is the mode probability from the previous time step, and \bar{c}_j is a normalizing constant.

Secondly, the mixing probabilities are used to calculate the mixed initial conditions for the state estimate and covariance, as shown in (36) and (37), respectively:

$$\hat{x}_{0j,k|k} = \sum_{i=1}^r \hat{x}_{i,k|k} \mu_{ij,k|k} \quad (36)$$

$$\hat{P}_{0j,k|k} = \sum_{i=1}^r \mu_{ij,k|k} \left\{ \hat{P}_{i,k|k} + (\hat{x}_{i,k|k} - \hat{x}_{0j,k|k})(\hat{x}_{i,k|k} - \hat{x}_{0j,k|k})^T \right\} \quad (37)$$

where $\hat{x}_{i,k|k}$ and $\hat{P}_{i,k|k}$ are the mode matched state and covariance estimate from the previous time step.

Thirdly, the computed initial conditions are used for mode-matched filtering. Simply put, they are used as inputs to each individual filter alongside the current measurements z_k and input u_k . Then, each filter provides an updated mode-matched state and covariance estimate, $\hat{x}_{i,k+1|k+1}$ and $\hat{P}_{i,k+1|k+1}$.

In the next step, a likelihood function based on the Gaussian assumption is defined for each filter, based on the mode-matched innovation and innovation covariance:

$$\Lambda_{j,k+1} = \mathcal{N}(z_k; \mathbf{v}_{j,k+1}, \mathbf{S}_{j,k+1}) \quad (38)$$

which can be computed as [43,44]:

$$\Lambda_{j,k+1} = \frac{1}{\sqrt{\det(2\pi|\mathbf{S}_{j,k+1}|_{ABS})}} \exp \left[-\frac{1}{2} \mathbf{v}_{j,k+1} \mathbf{S}_{j,k+1}^{-1} \mathbf{v}_{j,k+1} \right] \quad (39)$$

In the fifth step, the computed likelihoods are used to update the mode probabilities:

$$\mu_{j,k+1} = \frac{1}{c} \Lambda_{j,k+1} \bar{c}_j \quad (40)$$

$$c = \sum_{i=1}^r \Lambda_{j,k+1} \bar{c}_j \quad (41)$$

Finally, the output state and covariance are updated as a weighted sum of the mode-matched estimates and associated mode probabilities.

$$\hat{x}_{k+1|k+1} = \sum_{j=1}^r \hat{x}_{j,k+1|k+1} \mu_{j,k+1} \quad (42)$$

$$\hat{P}_{k+1|k+1} = \sum_{j=1}^r \mu_{j,k+1} \left\{ \hat{P}_{j,k+1|k+1} + (\hat{x}_{j,k+1|k+1} - \hat{x}_{k+1|k+1})(\hat{x}_{j,k+1|k+1} - \hat{x}_{k+1|k+1})^T \right\} \quad (43)$$

The algorithm outlined in this section is adopted in this study for the IMM SVSF-KF, with the SVSF and KF being the filters used in the third step.

4. Simulation results and discussion

The performances of our two newly proposed SVSF-KF approaches, which we call the NIS SVSF-KF and IMM SVSF-KF, are tested in experimental simulations involving the simple linear situation described in (28). A linear simulation is considered in order to provide a detailed comparison of the SVSF (sub-optimal but robust) with the KF (optimal) strategies. The methods could also be extended and applied on a nonlinear system or measurement. We consider two basic test scenarios, one with a permanent fault, and one with just a temporary fault.

In our simulations, we simulate the free response of a simple mass-spring-damper system. As in the previous simulation, after 30 seconds the mass suddenly increases from 15 kg to 35 kg, and the damping coefficient from 0.5 Ns/m to 2 Ns/m. Full measurements are available, and the measurement noise variance is 0.001 for both states. Otherwise, no significant process noise is considered. The sampling rate used for the simulation is $T = 1$ ms.

For the SVSF-based estimates, a smoothing boundary layer width vector is set based on trial-and-error tuning as:

$$\Psi = \begin{bmatrix} 1 \\ 0.2 \end{bmatrix} \quad (44)$$

For the VBL-based SVSF-KF, an SBL limit of 50 is used, based on the position state. For the NIS SVSF-KF, triggering thresholds of 140 for ‘‘on’’ and 120 for ‘‘off’’ were used. These values represent tail probabilities of 0.001 and 0.05, respectively, which correspond to a memory factor of $\alpha = 0.965$ and 92° of freedom as per (33). For the IMM SVSF-KF, initial mode probabilities of 0.95 for the KF and 0.05 for the SVSF were empirically determined. The mode transition probability matrix was set as:

$$p = \begin{bmatrix} 0.98 & 0.02 \\ 0.02 & 0.98 \end{bmatrix}$$

4.1. Case one: permanent fault

First under consideration is the performance of the filters upon the introduction of a permanent fault halfway through the simulation. The plots of the position and velocity state measurements and estimates are shown in Fig. 7 and Fig. 8, respectively. The filters under study include the original KF, SVSF and VBL-based SVSF-KF, as well as the newly proposed NIS and IMM variations of the SVSF-KF. For both the position and velocity states, it is clear that all of the filters under study manage to perform exceptionally well and can barely be differentiated from one another up until the introduction of the modeling change at 30 s. When the fault is introduced, there is significantly noticeable divergence in both state estimates by the KF and SVSF-KF. Both filters fail to demonstrate robustness, and the accuracy of their estimates show significant degradation in the presence of the fault. This behaviour is expected with the KF’s lack of robustness, and as for the SVSF-KF, can be attributed to high frequency gain switching phenomena described in earlier sections of this study. As for the SVSF, it is shown effectively track the states throughout the simulation, but as previously discussed, provides a suboptimal estimate prior to the fault. Finally, both the NIS and IMM SVSF-KF demonstrate effective tracking of both states throughout the entire simulation with no signs of difficulty or compromise in performance.

The gain activation of the NIS SVSF-KF is plotted in Fig. 9 for further examination of its switching performance. It can be seen in the figure that the NIS-based detection scheme can recognize and account for the fault shortly after its occurrence by switching to and maintaining the SVSF gain for the remainder of the simulation. In fact, the NIS-based approach detects the fault within approximately 2.3 s of its

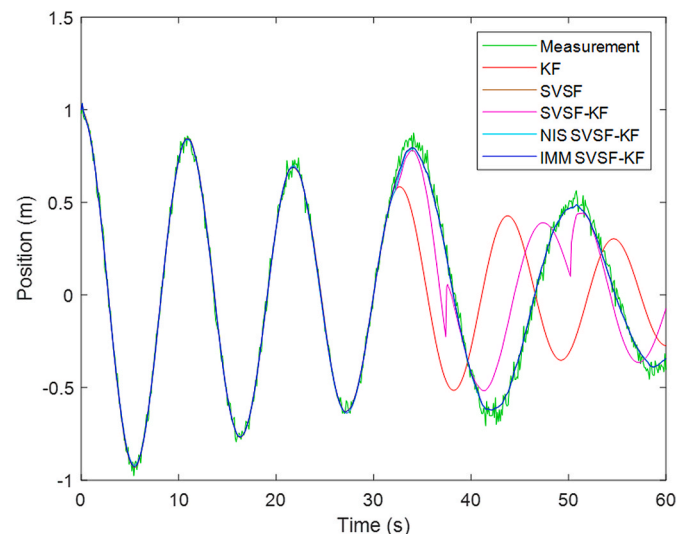


Fig. 7. Measurement and estimates of the position state (permanent fault).

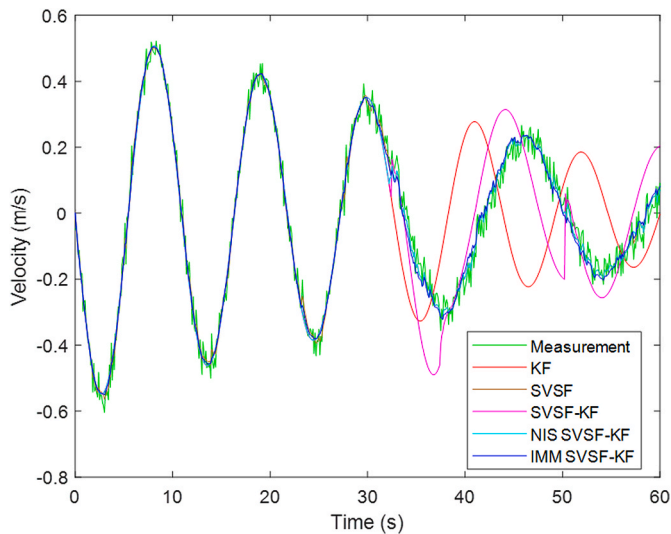


Fig. 8. Measurement and estimates of the velocity state (permanent fault).

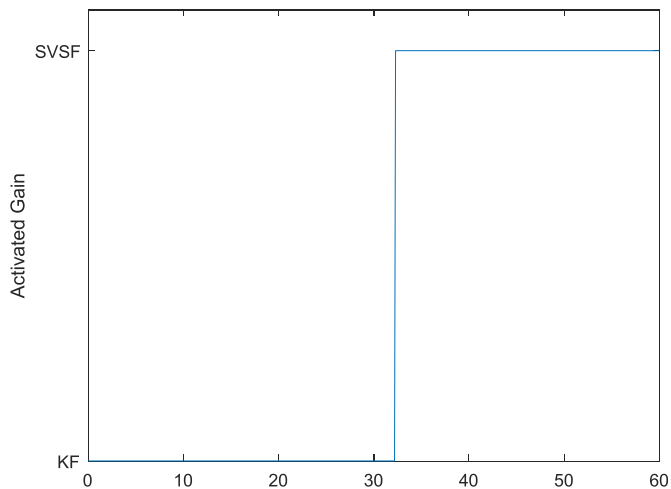


Fig. 9. NIS SVSF-KF gain activation plot (permanent fault).

occurrence. Furthermore, it can be observed that the NIS approach can maintain the SVSF gain and eliminate the high-frequency switching behaviour associated with the original SVSF-KF method. The actual NIS value of the position state across the entire simulation is plotted in Fig. 10, in which the red line indicates the “on” threshold for the SVSF gain activation, and the green line indicates the “off” threshold, further corroborating the validity and simplicity of the NIS.

The mode probabilities of the IMM SVSF-KF throughout the simulation are shown in Fig. 11. It can be seen from this figure that the IMM favours the KF prior to the fault’s occurrence, and then favours the SVSF upon the introduction of the fault. However, an overall combined weighting scheme is observed with the mode probabilities throughout the simulation. This combined weighting scheme is unlike the NIS approach, which outputs either a pure SVSF or KF estimate. Regardless, the IMM can detect the fault within 1.9 s, which is quicker than the 2.3 s taken by the NIS SVSF-KF. One issue that is readily apparent is the fact that the mode probabilities often remain close to the halfway point. Consequently, the less probable mode is significantly weighted and thus affecting the final output estimate. This may result in a less than optimal estimate by the IMM SVSF-KF.

The overall performance of each filter is compared by simulating 500 Monte Carlo runs of the scenario in study. The average RMSE of each filter for the position state estimate is recorded for three intervals of the

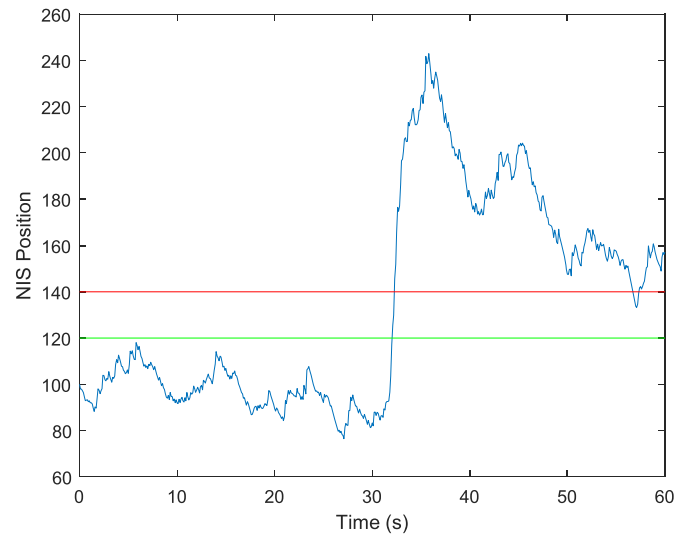


Fig. 10. NIS of the position state (permanent fault). Red and green lines indicate “on” and “off” thresholds for SVSF gain, respectively. (For interpretation of the references to colour in this figure legend, the reader is referred to the Web version of this article.)

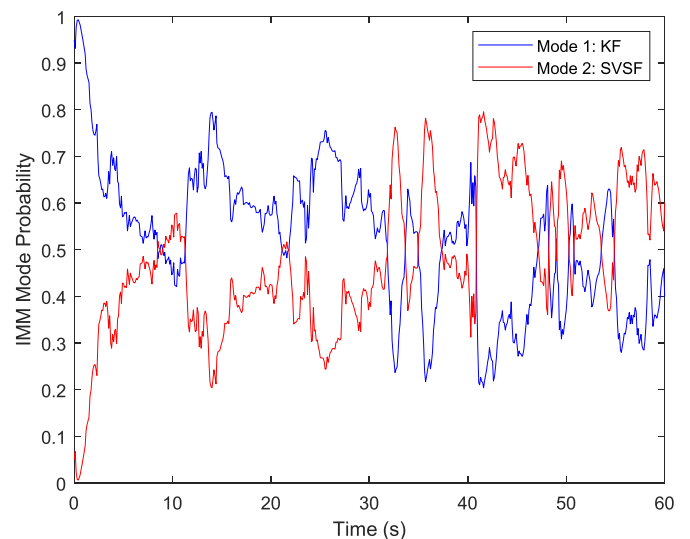


Fig. 11. IMM mode probability (permanent fault).

simulations: prior to the fault $t < 30s$, after the fault $t \geq 30s$, and throughout the entire simulation $0 \leq t \leq 60s$. The results of the first test case, where a permanent fault is introduced, are presented in Table 1.

It can be observed that the KF and SVSF-KF both perform poorly in the presence of the fault, despite having the best pre-fault performance. The NIS also has a pre-fault RMSE that is identical that of the optimal KF estimates. While the fault is introduced and after its conclusion, the IMM SVSF-KF has the best performance, with the NIS coming within fine margins in terms of performance. However, the IMM yields a suboptimal pre-fault estimate. The advantage of the NIS and IMM over the SVSF-KF is apparent in the fault stage. Whereas the advantage over the SVSF is

Table 1
RMSE results of various filters under permanent fault conditions.

Time	KF	SVSF	SVSF-KF	NIS SVSF-KF	IMM SVSF-KF
$t < 30s$	0.0030	0.0064	0.0030	0.0030	0.0057
$t \geq 30s$	0.4398	0.0265	0.1599	0.0273	0.0263
$0 \leq t \leq 60s$	0.3745	0.0218	0.1507	0.0225	0.0212

more obvious in the pre-fault phase.

In summary, the IMM SVSF-KF performs the best during the faulty conditions but provides a suboptimal estimate prior to the fault. The reverse is true with the NIS, which provides an optimal pre-fault estimate, and a robust estimate during the fault. Compared to the original VBL-based SVSF-KF, the NIS and IMM SVSF-KF represent an overall improvement in performance of 85.1 and 85.9%, respectively.

4.2. Case two: temporary fault

The next simulation considers a similar scenario to the one previously examined and discussed, except that the modeling change is temporary and resolved 30 s after its introduction. As in the previous trial, we plot the position and velocity and state estimates of each of the filters in Figs. 12 and 13, respectively.

Inspecting the plot of the position state estimates in Fig. 12, several observations can be made. Prior to the fault's incidence at 30 s, all filters exhibit the ability to accurately track the true state, with no discernible difference between any of the filters. Upon the introduction of the fault at 30 s, both the KF and the SVSF-KF can be seen diverging from the true state and failing to provide an accurate estimate. Upon the conclusion of the faulty conditions, the KF fails to recover to provide an optimal estimate, whereas the SVSF-KF is shown to recover after approximately 15 s. The SVSF, NIS SVSF-KF and IMM SVSF-KF, however, display no noticeable divergence and instead, qualitatively prove to accurately track the state throughout the entirety of the simulation. The velocity state estimates are consistent with the findings of the position state, with a slight exacerbation to both the KF and SVSF-KF's degradation in performance.

Fig. 14 shows the NIS SVSF-KF gain activation plot. In this figure, the NIS approach is evidently effective in rapidly detecting the onset and departure of the fault or modeling uncertainty. There is a 2.1 s delay in the detection of the

Fault until the SVSF gain is activated, and a subsequent 12.8 s delay from the fault's passing until the KF gain is activated. Regardless, the NIS SVSF-KF can maintain steady operation of the SVSF gain throughout the entirety of the fault's presence without any switching or chattering. In Fig. 15, the NIS values of the position state are shown, along with the mechanism behind the detection of system change. From this figure, the effectiveness of the gain activation scheme is further validated, especially in the rapidness of its detection of the fault. However, as already inferred, the NIS is somewhat slow in determining the fault's cessation. Approximately 10 s elapse before the NIS value crosses below the "off" threshold to switch to the KF gain. Thus, it may prove worthwhile for

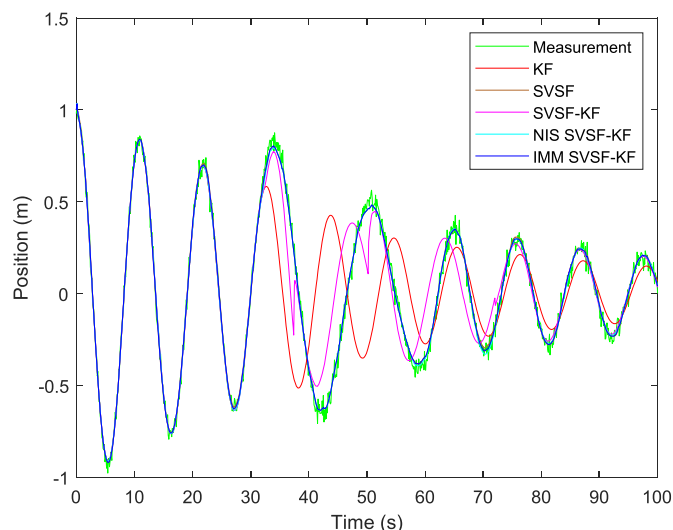


Fig. 12. Measurement and estimates of the position state (temporary fault).

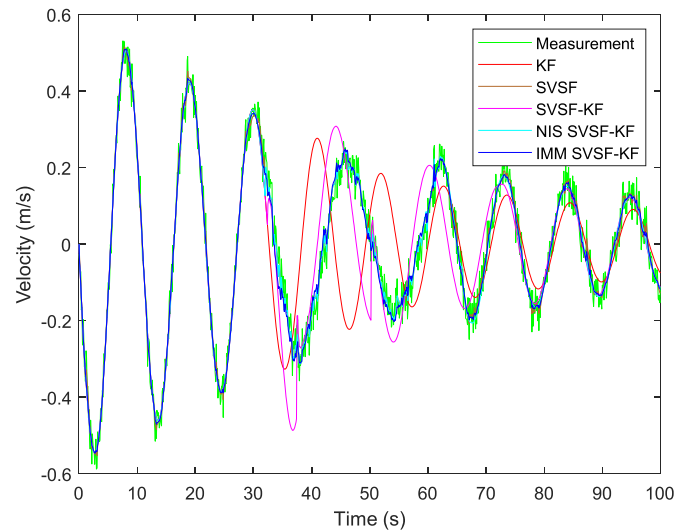


Fig. 13. Measurement and estimates of the velocity state (temporary fault).

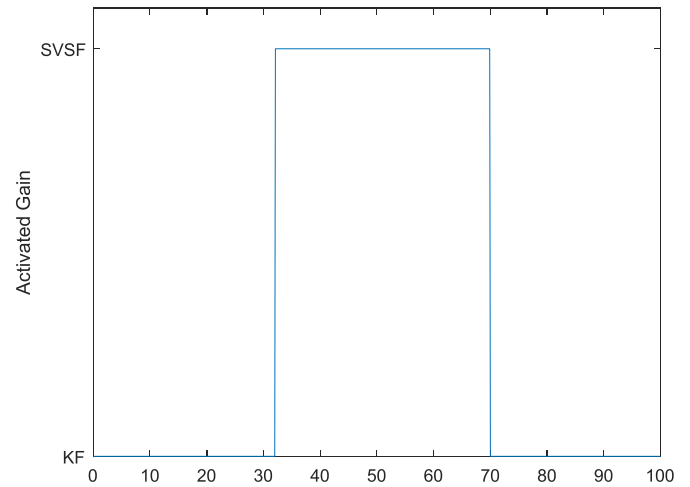


Fig. 14. NIS SVSF-KF gain activation plot (temporary fault).

future research effort and attention to be directed towards the adjustment of the NIS thresholds to further improve the performance of the approach in this regard. Albeit, careful consideration is required for this, as the risk of increased false positives or negatives is not negligible.

The mode probabilities as dictated by the IMM SVSF-KF are plotted in Fig. 16. From this figure, the IMM can be seen to have a combined weighting scheme for both filters. Despite the combined weighting, a clear trend is visible in the IMM's choice of the most probable mode. For example, during the period prior to the modeling change or fault's introduction, the KF mode is generally determined to be the heavier weighted filter operating. Upon the fault's introduction at 30 s, the SVSF becomes more heavily weighted, and subsequently, the KF is more dominant again upon the fault's exit at 60 s. While this combined weighting scheme may negatively impact the final weighted estimate, the IMM is superior to the NIS approach when it comes to the rapidness of detecting the onset and departure of the fault. The IMM SVSF-KF detects the modeling change with a delay of 1.9 s, compared to the 2.1 s by the NIS SVSF-KF. The conclusion of the fault is detected with a delay of 2.9 s by the IMM SVSF-KF, compared to a delay of 12.8 s by the NIS SVSF-KF.

As in the previous trials, 500 Monte Carlo runs of the scenario in study were carried out and the RMSE results of the.

Position estimates for all filters are recorded, as can be seen in

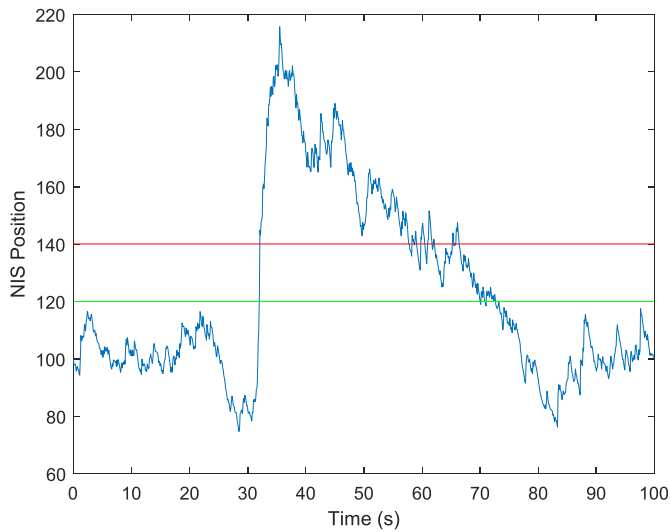


Fig. 15. NIS of the position state (temporary fault). Red and green lines indicate “on” and “off” thresholds for SVSF gain, respectively. (For interpretation of the references to colour in this figure legend, the reader is referred to the Web version of this article.)

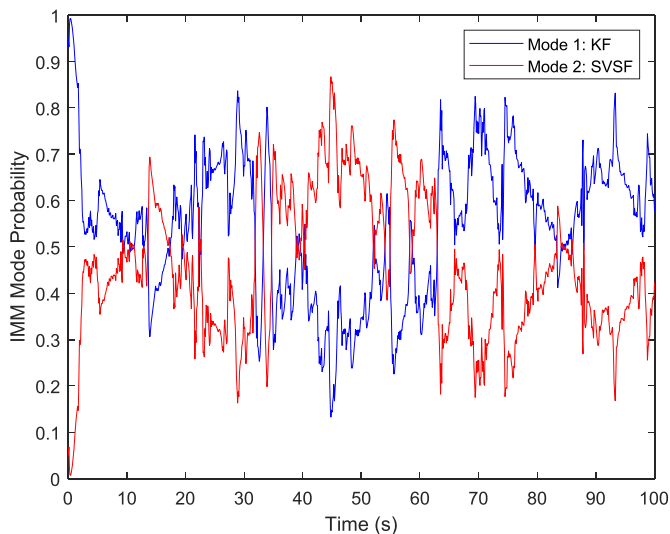


Fig. 16. IMM mode probability (temporary fault).

Table 2
RMSE results of various filters under temporary fault conditions.

Time	KF	SVSF	SVSF-KF	NIS SVSF-KF	IMM SVSF-KF
$t < 30s$	0.0027	0.0102	0.0027	0.0027	0.0073
$30 \leq t < 60s$	0.4406	0.0214	0.1570	0.0216	0.0213
$60 \leq t < 100s$	0.0646	0.0103	0.0617	0.0029	0.0070
$0 \leq t < 100s$	0.2937	0.0171	0.1335	0.0148	0.0152

Table 2. Note that this table also considers the RMSE value after the fault, where $60 \leq t \leq 100s$. From **Table 2**, it is clear that the KF performs

VI. Appendix: SVSF Proof of Stability

The smooth variable structure filter (SVSF) guarantees stability by making use of a Lyapunov stability condition. According to Lyapunov stability theory, a Lyapunov function V is said to be stable if V is locally positive definite and the time derivative of V is locally negative semi-definite. Let V be a Lyapunov function defined in terms of the SVSF *a posteriori* estimation error, such that:

the worst overall for the entire course of the simulation, followed by the SVSF-KF. Despite this, the KF demonstrates the lowest RMSE prior to the fault or modeling change, tied with both the SVSF-KF and the NIS SVSF-KF. The best overall performer is the NIS SVSF-KF, closely followed by the IMM SVSF-KF, and the SVSF.

It can thus be inferred that despite the NIS SVSF-KF’s slower response to detecting the start and end of the modeling change, it is still able to perform robustly enough to outperform all the other filters, including the IMM SVF-KF. Furthermore, it is interesting to observe that the IMM SVSF-KF fails to return the optimal KF estimate prior to the fault and after it concludes even when it is deemed to be the more probable filter. This can be explained by the IMM’s weighted final output scheme, and the fact that a mix of both filters is determined throughout the entire simulation, as previously observed in **Fig. 16**. This limitation of the IMM SVSF-KF may be mitigated in future studies by enforcing a condition to allocate the full weight to one filter if it is determined more probable, and a weight of zero to the other filter. Regardless, the IMM SVSF-KF yields the best results during the fault’s presence, but by a non-significant margin when compared with the NIS SVSF-KF. Overall, the NIS and IMM SVSF-KF represent an improvement of 88.9 and 88.6%, respectively, compared to the VBL-based SVSF-KF.

5. Conclusion

The results of our simulations demonstrate that the newly proposed NIS- and IMM-based SVSF-KF outperform the existing SVSF-KF approaches in detecting faults and reducing chatter. The NIS also has the benefit over the traditional SVSF of having the ability to provide an optimal estimate prior to the occurrence of a fault. Between the two newly proposed approaches, the NIS is considered more favourable due to its lower computational complexity despite performing with slightly less robustness as the IMM in the presence of a fault. However, further improvements to the NIS SVSF-KF may also be realized by future research directed towards a more careful approach to the tuning of the fading memory parameter and switching thresholds for more rapid detection of faults. Future work also includes the application of the proposed methods to a nonlinear system which is being built for experimentation.

Credit author statement

Jacob Goodman: Conceptualization, Methodology, Investigation, Writing – original draft. **Waleed Hilal:** Writing – original draft, Writing – review & editing, Visualization, Validation. **S. Andrew Gadsden:** Writing – review & editing, Supervision, Project administration, Funding acquisition, Conceptualization, Methodology. **Charles D. Eggleton:** Writing – review & editing, Supervision

Declaration of competing interest

The authors declare that they have no known competing financial interests or personal relationships that could have appeared to influence the work reported in this paper.

Data availability

No data was used for the research described in the article.

$$V = e_{z,k+1|k+1}^T e_{z,k+1|k+1} > 0 \tag{A.1}$$

According to Lyapunov stability theory, the estimation process is stable if the following is satisfied:

$$\Delta V \leq 0 \tag{A.2}$$

Where ΔV represents the change in the Lyapunov function, and in this case, is defined as follows:

$$\Delta V = e_{z,k+1|k+1}^T e_{z,k+1|k+1} - e_{z,k|k}^T e_{z,k|k} \tag{A.3}$$

Substitution of (A.3) into (A.2), and rearranging, yields the following

$$e_{z,k+1|k+1}^T e_{z,k+1|k+1} < e_{z,k|k}^T e_{z,k|k} \tag{A.4}$$

Equation (A.4) is equivalent to the following, which is the stability condition for the SVSF:

$$|e_{z,k+1|k+1}|_{Abs} < |e_{z,k|k}|_{Abs} \tag{A.5}$$

To remove the absolute operator in (A.5), both sides are expressed in the form of diagonal matrices (i.e., $diag(e)$), as follows:

$$\begin{aligned} &diag(e_{z,k+1|k+1})diag(e_{z,k+1|k+1}) \\ &< diag(e_{z,k|k})diag(e_{z,k|k}) \end{aligned} \tag{A.6}$$

Assuming that the measurement function is well-defined (and it may be linearized as C), then the *a posteriori* measurement error may be calculated as:

$$e_{z,k+1|k+1} = Ce_{x,k+1|k+1} + v_{k+1} \tag{A.7}$$

Substitution of (A.7) into (A.6) yields:

$$\begin{aligned} &\left(\begin{aligned} &diag(Ce_{x,k+1|k+1})diag(Ce_{x,k+1|k+1}) \\ &+diag(v_{k+1})diag(v_{k+1}) \\ &+diag(Ce_{x,k+1|k+1})diag(v_{k+1}) \\ &+diag(v_{k+1})diag(Ce_{x,k+1|k+1}) \\ &diag(Ce_{x,k|k})diag(Ce_{x,k|k}) \end{aligned} \right) \\ &< \left(\begin{aligned} &+diag(v_k)diag(v_k) \\ &+diag(Ce_{x,k|k})diag(v_k) \\ &+diag(v_k)diag(Ce_{x,k|k}) \end{aligned} \right) \end{aligned} \tag{A.8}$$

If the measurement noise v_{k+1} is stationary white, then by taking the expectation of both sides in (A.8) and simplifying yields the following:

$$\begin{aligned} &E \left[\begin{aligned} &diag(Ce_{x,k+1|k+1})diag(Ce_{x,k+1|k+1}) \\ &+diag(v_{k+1})diag(v_{k+1}) \end{aligned} \right] \\ &< E \left[\begin{aligned} &diag(Ce_{x,k|k})diag(Ce_{x,k|k}) \\ &+diag(v_k)diag(v_k) \end{aligned} \right] \end{aligned} \tag{A.9}$$

Where $E[diag(Ce_{x,k+1|k+1})diag(v_{k+1})]$ and $E[diag(v_k)diag(Ce_{x,k|k})]$ vanish due to the white noise assumption. For a diagonal, positive and time-invariant measurement matrix, (A.9) becomes:

$$\begin{aligned} &E[diag(e_{x,k+1|k+1})diag(e_{x,k+1|k+1})] \\ &< E[diag(e_{x,k|k})diag(e_{x,k|k})] \end{aligned} \tag{A.10}$$

Note that the assumptions pertaining to the measurement matrix are realistic since most applications use linear sensors as feedback in their operations. Moreover, these sensors are well calibrated and their structures are well-known. Finally, (A.10) becomes:

$$E(|e_{x,k+1|k+1}|_{Abs}) < E(|e_{x,k|k}|_{Abs}) \tag{A.11}$$

Equation (A.11) is the proof of stability for the SVSF. It states that the expectation of the *a posteriori* estimation error is reduced over time (i.e., converges towards a region of the state trajectory referred to as the existence subspace).

Furthermore, the proof of stability may be used to derive the SVSF gain K_{k+1}^{SVSF} . Define γ to be a diagonal matrix with elements $0 < \gamma_{ii} \leq 1$, such that:

$$|e_{z,k|k}|_{Abs} > \gamma |e_{z,k|k}|_{Abs} \tag{A.12}$$

Adding the absolute value of the *a priori* measurement error $|e_{z,k+1|k}|_{Abs}$ to both sides of (A.12) yields:

$$\begin{aligned} &|e_{z,k+1|k}|_{Abs} + |e_{z,k|k}|_{Abs} \\ &> |e_{z,k+1|k}|_{Abs} + \gamma |e_{z,k|k}|_{Abs} \end{aligned} \tag{A.13}$$

The absolute value of the measurement matrix multiplied with the SVSF gain $|CK_{k+1}^{SVSF}|_{Abs}$ is set equal to the right side of (A.13):

$$|CK_{k+1}^{SVSF}|_{Abs} = |e_{z,k+1|k}|_{Abs} + \gamma |e_{z,k|k}|_{Abs} \quad (\text{A.14})$$

Next, consider the following definition:

$$|CK_{k+1}^{SVSF}|_{Abs} = CK_{k+1}^{SVSF} \circ \text{sign}(CK_{k+1}^{SVSF}) \quad (\text{A.15})$$

Furthermore, the sign of the measurement matrix multiplied with the SVSF gain CK_{k+1}^{SVSF} is set equal to the sign of the *a priori* measurement error $e_{z,k+1|k}$. This leads to the SVSF gain (with a *sign* function), as follows:

$$K_{k+1}^{SVSF} = C^+ (|e_{z,k+1|k}|_{Abs} + \gamma |e_{z,k|k}|_{Abs}) \dots \dots \circ \text{sign}(e_{z,k+1|k}) \quad (\text{A.16})$$

Note that (A.16) satisfies and is derived from inequality (A.14), and for $0 < \gamma_{ii} \leq 1$ it satisfies (A.14) with the stability condition (A.5).

References

- [1] R.E. Kalman, A new approach to linear filtering and prediction problems, *Journal of Basic Engineering* 82 (1) (Mar. 1960) 35–45, <https://doi.org/10.1115/1.3662552>.
- [2] H.H. Afshari, S.A. Gadsden, S. Habibi, Gaussian filters for parameter and state estimation: a general review of theory and recent trends, *Signal Process.* 135 (2017), <https://doi.org/10.1016/j.sigpro.2017.01.001>.
- [3] Y. Shtessel, C. Edwards, L. Fridman, A. Levant, *Sliding Mode Control and Observation*, 2014, <https://doi.org/10.1007/978-0-8176-4893-0>.
- [4] S. Habibi, The smooth variable structure filter, *Proc. IEEE* 95 (5) (2007), <https://doi.org/10.1109/JPROC.2007.893255>.
- [5] M. Avzayesh, M. Abdel-Hafez, M. AlShabi, S.A. Gadsden, The smooth variable structure filter: a comprehensive review, *Digit. Signal Process.: A Review Journal* 110 (2021), <https://doi.org/10.1016/j.dsp.2020.102912>.
- [6] A. Šabanović, Variable structure systems with sliding modes in motion control - a survey, *IEEE Trans. Ind. Inf.* 7 (2) (2011), <https://doi.org/10.1109/TII.2011.2123907>.
- [7] S. Andrew Gadsden, M. Al-Shabi, A Study of Variable Structure and Sliding Mode Filters for Robust Estimation of Mechatronic Systems, 2020, <https://doi.org/10.1109/IEMTRONICS51293.2020.9216381>.
- [8] M. Al-Shabi, *The General Toeplitz/Observability SVSF*, McMaster University, Hamilton, Ontario, 2011.
- [9] M. Attari, S. Habibi, Automotive tracking technique using a new IMM based PDA-SVFSF, in: *ASME International Mechanical Engineering Congress and Exposition, Proceedings (IMECE)* vol. 12, 2014, <https://doi.org/10.1115/IMECE2014-36412>.
- [10] M. Attari, Z. Luo, S. Habibi, An SVSF-based generalized robust strategy for target tracking in clutter, *IEEE Trans. Intell. Transport. Syst.* 17 (5) (2016), <https://doi.org/10.1109/TITS.2015.2504331>.
- [11] F. Demim, A. Nemra, K. Louadj, Robust SVSF-slam for unmanned vehicle in unknown environment, *IFAC-PapersOnLine* 49 (2016) 21, <https://doi.org/10.1016/j.ifacol.2016.10.585>.
- [12] F. Demim, A. Nemra, K. Louadj, M. Hamerlain, A. Bazoula, A New Approach to Improve the Success and Solving the UGVs Cooperation for SLAM Problem, Using a SVSF Filter, 2016, <https://doi.org/10.1145/3038884.3038894>.
- [13] F. Demim, A. Nemra, K. Louadj, M. Hamerlain, A. Bazoula, Cooperative SLAM for multiple UGVs navigation using SVSF filter, *Automatika* 58 (2017) 1, <https://doi.org/10.1080/00051144.2017.1372123>.
- [14] F. Outamazirt, L. Yan, F. Li, A. Nemra, Comparing between the performance of SVSF with EKF and NH ∞ for the autonomous airborne navigation problem, *IEEE Aerospace Conference Proceedings 2016-June* (2016), <https://doi.org/10.1109/AERO.2016.7500504>.
- [15] J. Goodman, J. Kim, A.S. Lee, S.A. Gadsden, M. Al-Shabi, A variable structure-based estimation strategy applied to an RRR robot system, *Journal of Robotics, Networking and Artificial Life* 4 (2017) 2, <https://doi.org/10.2991/jrnal.2017.4.2.8>.
- [16] S.A. Gadsden, T. Kirubarajan, Development of a variable structure-based fault detection and diagnosis strategy applied to an electromechanical system, in: *Signal Processing, Sensor/Information Fusion, and Target Recognition XXVI* vol. 10200, 2017, <https://doi.org/10.1117/12.2262570>.
- [17] M. Alshabi, A. Elnady, Recursive smooth variable structure filter for estimation processes in direct power control scheme under balanced and unbalanced power grid, *IEEE Syst. J.* 14 (1) (2020), <https://doi.org/10.1109/JSYST.2019.2919792>.
- [18] M. Avzayesh, M.F. Abdel-Hafez, W.M.F. Al-Masri, M. Alshabi, A.H. El-Hag, A hybrid estimation-based technique for partial discharge localization, *IEEE Trans. Instrum. Meas.* 69 (2020) 11, <https://doi.org/10.1109/TIM.2020.2999165>.
- [19] F. Demim, S. Benmansour, N. Abdelkrim, A. Rouigueb, M. Hamerlain, A. Bazoula, Simultaneous localisation and mapping for autonomous underwater vehicle using a combined smooth variable structure filter and extended kalman filter, *J. Exp. Theor. Artif. Intell.* (2021), <https://doi.org/10.1080/0952813X.2021.1908430>.
- [20] Y. Tian, H. Suwoyo, W. Wang, L. Li, An ASVFSF-SLAM algorithm with time-varying noise statistics based on MAP creation and weighted exponent, *Math. Probl Eng.* 2019 (2019), <https://doi.org/10.1155/2019/2765731>.
- [21] F. Demim, et al., A New Adaptive Smooth Variable Structure Filter SLAM Algorithm for Unmanned Vehicle, 2017, <https://doi.org/10.1109/ICoSC.2017.7958664>.
- [22] S. Rahimifard, S. Habibi, G. Goward, J. Tjong, Adaptive smooth variable structure filter strategy for state estimation of electric vehicle batteries, *Energies* 14 (2021) 24, <https://doi.org/10.3390/en14248560>.
- [23] Y. Chen, L. Xu, G. Wang, B. Yan, J. Sun, An improved smooth variable structure filter for robust target tracking, *Rem. Sens.* 13 (2021) 22, <https://doi.org/10.3390/rs13224612>.
- [24] F. Demim, A. Boucheloukh, A. Nemra, E. Kobzili, M. Hamerlain, A. Bazoula, An adaptive SVSF-SLAM algorithm in dynamic environment for cooperative unmanned vehicles, *IFAC-PapersOnLine* 52 (2019) 15, <https://doi.org/10.1016/j.ifacol.2019.11.707>.
- [25] F. Demim, A. Nemra, A. Boucheloukh, E. Kobzili, M. Hamerlain, A. Bazoula, SLAM based on adaptive SVSF for cooperative unmanned vehicles in dynamic environment, *IFAC-PapersOnLine* 52 (2019) 8, <https://doi.org/10.1016/j.ifacol.2019.08.051>.
- [26] H.H. Afshari, M. Attari, R. Ahmed, A. Delbari, S. Habibi, T. Shoa, Reliable state of charge and state of health estimation using the smooth variable structure filter, *Control Eng. Pract.* 77 (2018), <https://doi.org/10.1016/j.conengprac.2018.04.015>.
- [27] H. Zhou, L. Xu, W. Chen, K. Guo, F. Shen, Z. Guo, A novel robust filtering strategy for systems with Non-Gaussian noises, *AEU - International Journal of Electronics and Communications* 97 (2018), <https://doi.org/10.1016/j.aue.2018.10.004>.
- [28] Y. Liu, C. Wang, A FastSLAM Based on the Smooth Variable Structure Filter for UAVs, 2018, <https://doi.org/10.1109/URAI.2018.8441876>.
- [29] W. Li, H. Gu, W. Su, Partitioned Time-Varying Smooth Variable Structure Filter for Airport Target Tracking, 2017, <https://doi.org/10.1109/RADAR.2016.8059444>.
- [30] F. Outamazirt, L. Fu, Y. Lin, N. Abdelkrim, A new SINS/GPS sensor fusion scheme for UAV localization problem using nonlinear SVSF with covariance derivation and an adaptive boundary layer, *Chin. J. Aeronaut.* 29 (2) (2016), <https://doi.org/10.1016/j.cja.2016.02.005>.
- [31] M. Al-Shabi, M. Bani-Yonis, K.S. Hatamleh, The Sigma-point Central Difference Smooth Variable Structure Filter Application into a Robotic Arm, 2015, <https://doi.org/10.1109/SSD.2015.7348201>.
- [32] A.S. Lee, S.A. Gadsden, S.A. Wilkerson, An Adaptive Smooth Variable Structure Filter Based on the Static Multiple Model Strategy, 2019, <https://doi.org/10.1117/12.2519771>.
- [33] S.A. Gadsden, S.R. Habibi, A New Form of the Smooth Variable Structure Filter with a Covariance Derivation, 2010, <https://doi.org/10.1109/CDC.2010.5717397>.
- [34] S. Gadsden, *Smooth Variable Structure Filtering: Theory and Applications*, McMaster University, Hamilton, Ontario, 2011.
- [35] H. Suwoyo, et al., Maximum likelihood estimation-assisted ASVFSF through state covariance-based 2D SLAM algorithm, *Telkomnika (Telecommunication Computing Electronics and Control)* 19 (1) (2021), <https://doi.org/10.12928/TELKOMNIKA.V19I1.16223>.
- [36] M. Al-Shabi, S. Habibi, New Novel Time-Varying and Robust Smoothing Boundary Layer Width for the Smooth Variable Structure Filter, 2013, <https://doi.org/10.1109/ISMA.2013.6547375>.
- [37] S.A. Gadsden, S. Habibi, T. Kirubarajan, Kalman and smooth variable structure filters for robust estimation, *IEEE Trans. Aero. Electron. Syst.* 50 (2) (2014), <https://doi.org/10.1109/TAES.2014.110768>.
- [38] M. Al-Shabi, K.S. Hatamleh, The unscented smooth variable structure filter application into a robotic arm, *ASME International Mechanical Engineering Congress and Exposition, Proceedings (IMECE)* 4B (2014), <https://doi.org/10.1115/IMECE2014-40118>.
- [39] H. Zhou, Y. Xia, Y. Deng, A new particle filter based on smooth variable structure filter, *Int. J. Adapt. Control Signal Process.* 34 (1) (2020), <https://doi.org/10.1002/acs.3067>.
- [40] W. Chen, H. Zhou, F. Shen, Z. Guo, Current statistic model and adaptive tracking algorithm based on Kalman and Smooth Variable Structure Filters, in: *9th International Conference on Microwave and Millimeter Wave Technology, ICMMT 2016 - Proceedings* vol. 2, 2016, <https://doi.org/10.1109/ICMMT.2016.7762534>.
- [41] W. Youn, S. Andrew Gadsden, Combined quaternion-based error state kalman filtering and smooth variable structure filtering for robust attitude estimation, *IEEE Access* 7 (2019), <https://doi.org/10.1109/ACCESS.2019.2946609>.
- [42] B.M. Dyer, T.R. Smith, S.A. Gadsden, M. Biglarbegian, Filtering Strategies for State Estimation of Omnivheel Robots, 2020, <https://doi.org/10.1109/ICMA49215.2020.9233826>.

- [43] Y. Bar-Shalom, X.-R. Li, T. Kirubarajan, Estimation with Applications to Tracking and Navigation, 2001, <https://doi.org/10.1002/0471221279>.
- [44] M.S. Grewal, A.P. Andrews, Kalman Filtering: Theory and Practice with MATLAB®, fourth ed., vol. 9781118851210, 2014, <https://doi.org/10.1002/9781118984987>.
- [45] P.S. Maybeck, Stochastic models, estimation, and control - Introduction, in: Stochastic Models, Estimation, and Control vol. 1, 1979.
- [46] H.A.P. Blom, Y. Bar-Shalom, The interacting multiple model algorithm for systems with markovian switching coefficients, IEEE Trans. Automat. Control 33 (8) (1988), <https://doi.org/10.1109/9.1299>.
- [47] S.A. Gadsden, M. el Sayed, S.R. Habibi, Derivation of an Optimal Boundary Layer Width for the Smooth Variable Structure Filter, 2011, <https://doi.org/10.1109/acc.2011.5990970>.
- [48] H.H. Afshari, S.A. Gadsden, S. Habibi, A nonlinear second-order filtering strategy for state estimation of uncertain systems, Signal Process. 155 (2019), <https://doi.org/10.1016/j.sigpro.2018.09.036>.
- [49] D. Simon, Optimal State Estimation: Kalman, H_{∞} , and Nonlinear Approaches, 2006, <https://doi.org/10.1002/0470045345>.
- [50] M. Spiller, D. Söffker, On the relation between smooth variable structure and adaptive kalman filter, Frontiers in Applied Mathematics and Statistics 6 (2020), <https://doi.org/10.3389/fams.2020.585439>.
- [51] J. Goodman, S.A. Wilkerson, C. Eggleton, S.A. Gadsden, A Multiple Model Adaptive SVSF-KF Estimation Strategy, 2019, <https://doi.org/10.1117/12.2520018>.
- [52] A. Gelb, Applied optimal estimation 64 (4) (2001).
- [53] Y. Qin, Y. Liang, Y. Yang, F. Yang, X. Wang, A Nonlinear Filter Switch Method Based on Normalized Innovation Square, 2013.
- [54] H. Musoff, P. Zarchan, Fundamentals of Kalman Filtering: A Practical Approach, third ed., 2009, <https://doi.org/10.2514/4.867200>.
- [55] R.G. Brown, P.Y.C. Hwang, Introduction to Random Signals and Applied Kalman Filtering, vol. 4, 1997.
- [56] A.F. Genovese, The interacting multiple model algorithm for accurate state estimation of maneuvering targets, Johns Hopkins APL Tech. Dig. 22 (4) (2001).